Journal of Materials Science: Materials in Electronics (2019) 30:3365–3377
https://doi.org/10.1007/s10854-018-00610-4

Preparation of microwave absorbing Co-C nanofibers with robust superhydrophobic properties by electrospinning

Yongqian Shen[1] · Yupeng Wei[1,2] · Jian Li[3] · Qinglin Li[1] · Jiqiang Ma[1] · Pingbo Wang[1] · Bin Li[1] · Wenbo He[1] · Xueyan Du[1]

Received: 29 October 2018 / Accepted: 19 December 2018 / Published online: 23 January 2019

Abstract

High-performance microwave absorbers with excellent absorption ability and superhydrophobic property are extremely significant for the application of stealthy techniques, especially in high-humidity environment. In this research, high-performance Co-C nanofibers (NFs) were prepared via electrospinning mathod by using of poly (vinyl alcohol) (PVA) and Cobalt acetate tetrahydrate (CoAc) solution as precursor with subsequent PVA pyrolyzation and carbonization process. The electromagnetic (EM) parameters and microwave absorption performance of the prepared NFs were investigated with the microwave frequency ranging from 2.0 GHz to 18.0 GHz. Analysis and comparison were performed on the impedance matching and loss mechanisms of each sample. The experimental results indicated that the sample calcinated at 950 °C achieved an optimal reflection loss (RL) of − 33.1 dB and an effective frequency bandwidth of 4.1 GHz under a thickness of 1.5 mm; and that the Co-C NFs membrane with the optimal absorption performance exhibited superhydrophobic property with a contact angle (CA) of 152°, suggesting their promising application to water-resistant stealthy materials.

1 Introduction

Recently, with the increasingly extensive applications of all kinds of electronic instruments, EM interference has posed the military and civilian applications at risks, which will influence the normal function of electronic devices and pose human health at risks. Therefore, there is an increasing demand to prepare high-performance EM wave absorbers featured by broad bandwidth, small thickness, light weight, and strong absorption performance [1–6].

Normally, EM wave absorbers are categorized into two types according to their material properties, i.e. dielectric loss materials and magnetic loss materials. Dielectric loss materials, including SiC [7], SnO_2 [8], CuO [9], MnO_2 [10], TiO_2 [11], ZnO [12], CuS [13], ZrO_2 [14], carbon-based materials [15] and conducting polymer [16] possess strong EM attenuation performance as a result of large dielectric loss angle tangent. Nevertheless, single dielectric loss materials are featured by high complex permittivity and low magnetic permeability, thereby causing impedance mismatch and restricting their application to microwave absorption. On the other hand, magnetic loss materials, e.g. Ni [17], Co [18], Fe [19], as well as their oxides [20–22], are able to greatly weaken the high-frequency skin effect and achieve the effective absorption of EM waves. However, the extensive applications of such materials are limited by their low stability in environment, large density and high reflection coefficient between their interfaces. Therefore, it is potentially an effective approach to fabricate composites by combining magnetic loss with dielectric loss to widen absorption bandwidth, enhance absorption intensity, and improve impedance matching.

Yongqian Shen and Yupeng Wei have contributed equally to this work.

✉ Xueyan Du
duxy@lut.cn

[1] State Key Laboratory of Advanced Processing and Recycling of Non-ferrous Metals, Key Laboratory of Nonferrous Metal alloys and Processing, Ministry of Education, School of Materials Science & Engineering, Lanzhou University of Technology, Lanzhou 730050, People's Republic of China

[2] Key Laboratory of Magnetism and Magnetic Materials of the Ministry of Education, Lanzhou University, Lanzhou 730000, People's Republic of China

[3] College of Chemistry and Chemical Engineering, Northwest Normal University, Lanzhou 730070, People's Republic of China

Recently, there is an increasing interest in carbon-based composites consisting of both carbon and magnetic components due to their good performance as microwave absorbers. Carbon-based composites are able to produce a variety of forms of EM losses, and avoid the large specific gravity of magnetic materials. Currently, researchers have developed some carbon-based materials as microwave absorbers, e.g. carbon nanotubes (CNTs) [23], MOF-derived carbon nanocubes [24], graphene (G) [25], carbon nanofibers (CNFs) [26] and carbon nanocoils (CNCs) [27]. Zhang et al. produced 1D porous Ni@C nanorods using a self-template method [28]. Liu et al. prepared Co/C nanoparticles in a mixed atmosphere of argon and methane using arc plasma method [29]. However, the preparation of EM absorbing materials using the electrospinning method is rarely reported, especially carbon–metal NFs.

In practical applications, EM wave absorbers are usually used in the environment featured by high humidity, harsh alkaline or acidic ambient, which reduces the conductivity of absorbers and further the EM wave absorption performance. Hence, microwave absorbers are required to have excellent water-resistant property. Commonly, superhydrophobic surfaces with water CA > 150° are considered to have excellent water-resistant property, enabling the quick removal of water from surface to maintain the conductivity of materials. Previous researchers have made great efforts on this field. For instance, Lu et al. reported that the carbon nanotubes composites modified by Fe_3O_4 nanopearls exhibited excellent microwave absorption performance and superhydrophobic properties [30]. Li et al. prepared that polyvinylidene fluoride/Fe_3O_4@polypyrrole NFs with the minimum RL reaching −21.5 dB at 16.8 GHz under a thickness of 2.5 mm by electrospinning exhibited superhydrophobic and self-healing properties [31]. Nevertheless, less attention has been paid to the fabrication of superhydrophobic EM wave absorbers using electrospinning method. As a result, the preparation of high-performance EM wave absorbers with excellent water-resistant property is of great significance.

In this work, we have successfully fabricated superhydrophobic Co-C NFs by electrospinning method, where their morphological and structural patterns were artificially controlled to reach the desired ones. The Co-C NFs were prepared by calcining the PVA-based NFs which were produced by the electrospinning of CoAc and PVA/H_2O solution. In the calcination process, the CoAc was steadily converted into new Co oxides and Co salts and then into Co nanoparticles in a strong reduction atmosphere formulated by PVA pyrolysis. The formed Co nanoparticles were planted in carbon-based NFs in a random manner in the carbonization process and mostly parceled by highly-oriented graphite layers. As a result of carbon protection, the products exhibited excellent physical and chemical stability. The prepared Co-C NFs had three advantages. Firstly, a "conductive network" was formed due to the fibrous morphology of the CNFs, and their density was reduced owing to the existence of carbon components; Secondly, the combination of dielectric CNFs and magnetic Co nanoparticles acquired good impedance matching by adjusting the EM parameters of the NFs; Finally, the low surface free energy of carbon and the rough structure formulated by Co nanoparticles contributed to the superhydrophobic property. Hence, the prepared lightweight Co-C NFs are a promising candidate for multi-functional water-resistant stealthy materials.

2 Experimental

2.1 Materials

Poly (vinyl alcohol) (PVA) with MW of 67000 g/mol was obtained from Shanghai Aladdin Reagent Inc., China. Cobalt acetate tetrahydrate (CoAc, 98%) was purchased from Xilong Chemical Co., Ltd., China. All the reagents used in this research were of analytical grade and were not further refined.

2.2 Preparation of Co-C NFs

The NFs were produced using traditional sol–gel method. The precursor of Co salt solution was prepared as follows. 4.25 mL of distilled water and 0.45 g of PVA were added into a flask, followed by the magnetic stirring at 80 °C for 1.5 h to guarantee the complete dissolving of the PVA. After that, 0.3 g of CoAc was added into the as-prepared product and the mixture was magnetically stirred at 50 °C for 2 h, followed by being stirred at ambient temperature for 13 h. The precursor solution was delivered to a stainless steel needle at a rate of 0.30 mL/h by a syringe pump. The needle was connected to a high-voltage power supply. In this research, the supply voltage was 15 kV and the distance between the syringe needle and the grounding collector (stainless steel wire mesh) was 12 cm.

The prepared fibrous membranes were dried at a temperature of 60 °C for 12 h. The PVA was pyrolyzed and the carbothermic reduction of Co^{2+} was carried out in vacuum as follows: (1) heated to 300 °C at a rate of 2.5 °C min^{-1}, and kept for 1 h to stabilize the morphology of the NFs; (2) further heated to an appropriate temperature at a rate of 2.5 °C min^{-1} and kept for 1 h to make the NFs composites carbonized, thereby acquiring high degree crystallinity Co. Then, the obtained NFs were naturally cooled to ambient temperature in vacuum. To improve the EM wave absorption performance, different calcination temperatures (550 °C, 750 °C and 950 °C) were adopted and the corresponding samples were labeled as S550, S750 and S950, respectively.

2.3 Characterizations

The micromorphology of the prepared product was observed by a field emission scanning electron microscope (FESEM, JSM-6700F, JEOL, Japan) and a transmission electron microscope (TEM, JEM-2100, JEOL, Japan) equipped with a high angle annular dark field scanning transmission electron microscope (HAADF-STEM) and an energy-dispersive X-ray spectroscope (EDX, Oxford Instrument, UK). Phase analysis was performed by an X-ray diffraction instrument (XRD, D8 ADVANCE, BRUKER AXS, Germany) using monochromatic Cu-Kα radiation ($\lambda = 1.5418$ Å) at a voltage of 40 kV and a current of 40 mA from 20° to 90° (2θ) with a scanning step of 10° min. The Raman spectra were obtained by a confocal Raman system (LabRAM HR Evolution, HORIBA, France) with a diode laser excitation of 532 nm at room temperature. A vibrating sample magnetometer (VSM, 7307, Lake Shore Cryotronics, US) was used to obtain the hysteresis loop. The contact angle (CA) was obtained using a CA measuring apparatus (SL200KB, Kino industry, US) with a droplet of 5 μL each time. The CA values of at least three points were averaged.

For the convenience of the measurement of EM parameters, the products were mixed with 90 wt% paraffin and 10 wt% Co-C NFs, followed by being pressed into a cylindrical compact with inner and outer diameters of 3.04 mm and 7.00 mm, respectively. Using transmission/reflection method, the complex permeability and permittivity of the product were measured using a vector network analyzer (N5244A, Agilent, US) at a frequency of 2.0–18.0 GHz.

3 Results and discussion

Scheme 1 presents the fabricating procedures of Co-C NFs. Firstly, a homogeneous solution was prepared by dissolving CoAc into PVA solution. The CoAc/PVA NFs were prepared using the electrospinning method. Secondly, the prepared CoAc/PVA NFs were calcined at an appropriate temperature in vacuum, in which the carbothermal reduction of Co^{2+} was occurred and the Co^{2+} was transformed into Co nanocrystals which were randomly distributed in the carbon framework. Finally, the Co-C NFs were prepared. The following reactions have been used to explain the formation of Co-C NFs [32]:

$$\mathrm{PVA} \rightarrow \mathrm{C} + \mathrm{CO} \tag{1}$$

$$\mathrm{Co(CH_3COO)_2 \cdot 4H_2O} \rightarrow \mathrm{Co(OH)(CH_3COO)} + \mathrm{CH_3COOH} + \mathrm{3H_2O} \tag{2}$$

$$\mathrm{Co(OH)(CH_3COO)} \rightarrow \mathrm{0.5CoCO_3} + \mathrm{0.5CoO} + \mathrm{0.5CH_3COCH_3} + \mathrm{0.5H_2O} \tag{3}$$

$$\mathrm{CoCO_3} \rightarrow \mathrm{CoO} + \mathrm{CO_2} \tag{4}$$

$$\mathrm{CoO} + \mathrm{CO\ or\ C} \rightarrow \mathrm{Co} + \mathrm{CO_2} \tag{5}$$

3.1 Morphology and crystalline phase

Figure 1 shows the SEM images of S550, S750 and S950. According to Fig. 1, the calcined NFs membranes present random and nonwoven mesh structures with large aspect ratio and a mean diameter of 150 nm. The inset of Fig. 1 clearly reveals the surface morphology of the calcined NFs

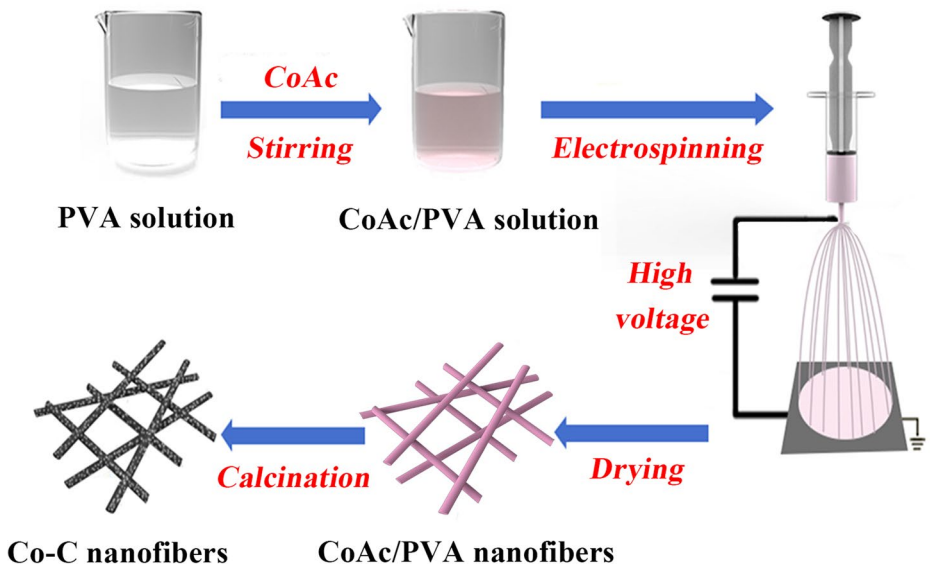

Scheme 1 Schematic of the fabrication procedure of Co-C NFs

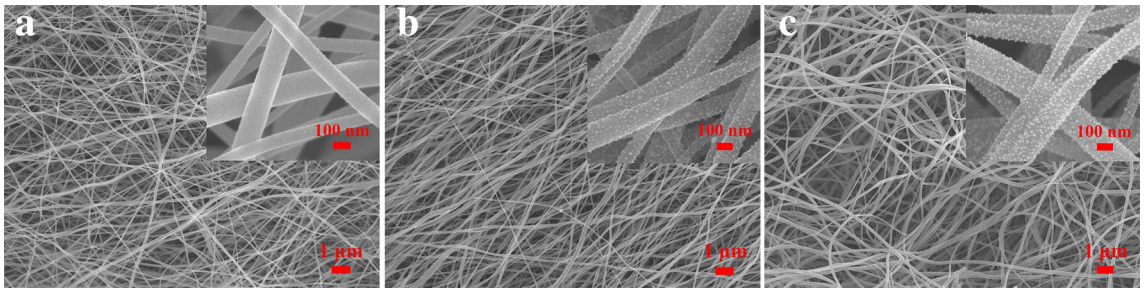

Fig. 1 SEM images of S550 (**a**), S750 (**b**) and S950 (**c**), insets show the high magnification of simples

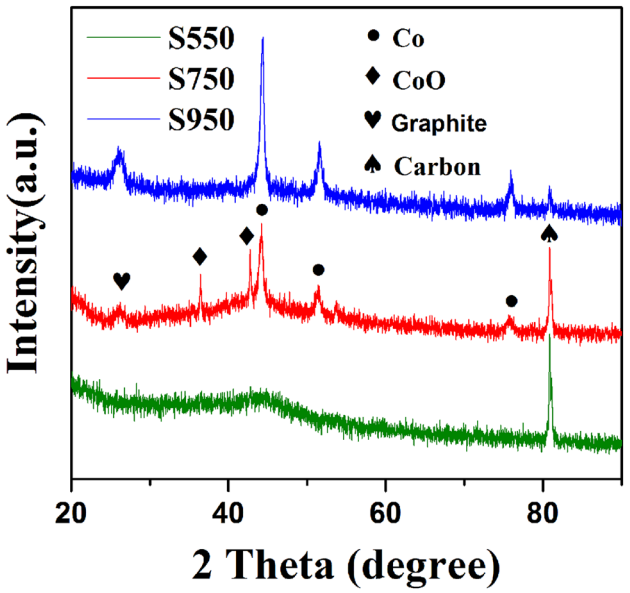

Fig. 2 XRD patterns of S550, S750 and S950

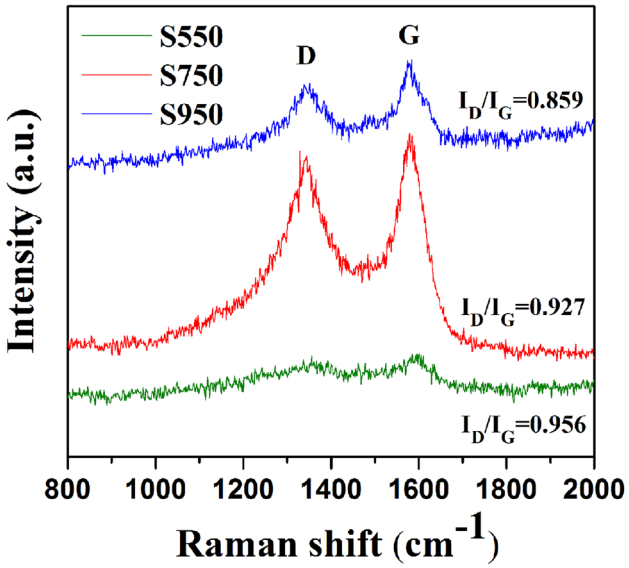

Fig. 3 Raman spectrum of S550, S750 and S950

membranes. For S550, the nanoprotrusions on the surface of the NFs are not obvious. For S750 and S950, the surfaces become very rough, with massive nanoprotrusions distributed on the surface. The inset of Fig. 1 indicates that more nanoprotrusions are formed on the surfaces of the NFs with the carbonization temperature increasing.

The crystallographic structures of S550, S750 and S950 were observed using an X-ray diffractometer. According to Fig. 2, there are three characteristic diffraction peaks at the positions of 44.2°, 51.5° and 75.6°, which correspond to the Co FCC crystal planes of (1 1 1), (2 0 0) and (2 2 0) (PDF#15–0806), respectively. The characteristic diffraction peak located at 25.2° corresponds to the graphite crystal plane of (0 0 2) (PDF#41-1487). The graphite was generated with the graphitization of PVA in vacuum under the catalysis of Co [32]. The characteristic peaks at 36.6° and 42.4° are attributed to the crystal planes of (1 1 1) and (2 0 0) of CoO (PDF#48-1719), respectively. It can be seen that the diffraction peak of CoO almost disappears at the carbonization temperature of 950 °C, indicating the near non-presence of crystallographic CoO in S950. There is an abnormal diffraction peak at the position of 81.3°, which also appeared in our previous research on nickel-carbon NFs [33], might result from the carbon crystal plane of (1 0 22) (PDF#50-1085). Besides, the characteristic diffraction peaks of CoO and Co are not observed for S550, indicating that the crystalline CoO and Co had not been formed at the carbonization temperature of 550 °C.

Figure 3 displays the Raman spectra of S550, S750 and S950. For all samples, the main peaks of 1580 cm^{-1} (G band) and 1340 cm^{-1} (D band) indicate the successful decomposition and conversion of PVA into carbon after the calcination process. The G band is caused by the stretching vibration of the sp^2 bond produced from sp^2 sites in graphitic carbon while the D band corresponds to the amorphous sp^3 carbon. Thus, the evaluation of the degree of graphitization can be conducted with I_G/I_D value as the reference [29]. In our experiment, the I_G/I_D values of

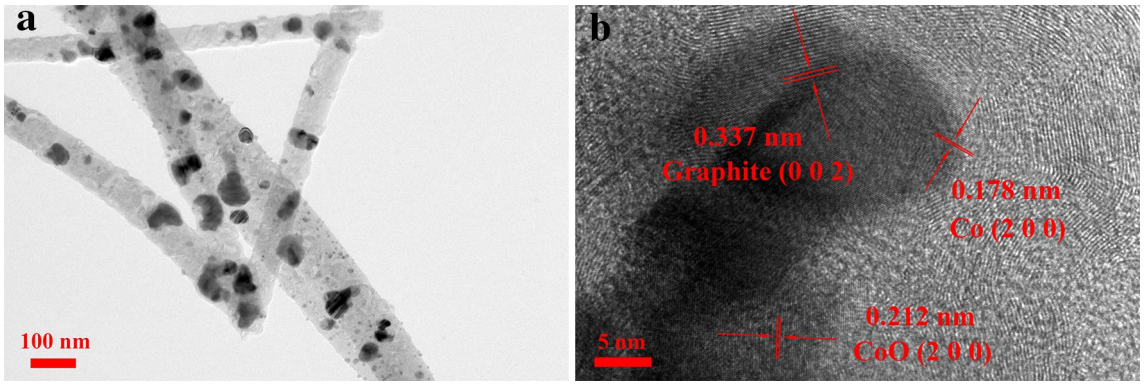

Fig. 4 TEM images of S750 (**a**); HRTEM images of S750 (**b**)

S550, S750 and S950 are 0.956, 0.927 and 0.859, respectively, indicating that the graphitization of the Co-C NFs is increased with the increase of the calcination temperature.

Figure 4 presents the TEM and HRTEM images of S750, from which the distribution and phase characteristics of Co nanoprotrusions in the Co-C NFs could be determined. Figure 4a displays the morphology and distribution of the Co nanoprotrusions, indicating the uniform distribution of the Co nanoprotrusions along the nanofibers. Figure 4b indicates that the Co particle is enclosed in a nanofiber with some graphite and amorphous carbon surrounding. The lattice spacing of 0.178 nm corresponds to the Co crystal plane of (2 0 0) and coincides well with the XRD pattern of FCC Co. The lattice spacing of 0.337 nm assigns to the graphite crystal plane of (0 0 2). The lattice spacing of 0.212 nm corresponds to the CoO crystal plane of (2 0 0). In addition, the Co particles are surrounded by several graphene layers, resulting from the catalytic effect of Co on the graphitization [24, 32].

The distribution of Co nanoparticles on the Co-C NFs was also verified by HAADF-STEM and STEM elemental mapping analysis, as observed in Fig. 5. It can be found from Fig. 5a that the distribution of Co nanoparticles is mainly determined by the atomic number and material thickness. In addition, a pure phase appears and the monodispersed Co nanoparticles are scattered in the NFs in a random manner. The EDS Co mapping is exhibited in Fig. 5b, it can be clearly observed that the Co nanoparticles with a diameter of about 20 nm are uniformly monodispersed and scattered on the surface along the Co-C NFs. The EDS elemental mappings of C and O confirm a uniform distribution in the Co-C NFs.

3.2 Static magnetic properties

Figure 6 exhibits the hysteresis loops of the three samples. For S550, the saturation magnetization state is not achieved in the external magnetic field of 9500 Oe, indicating the

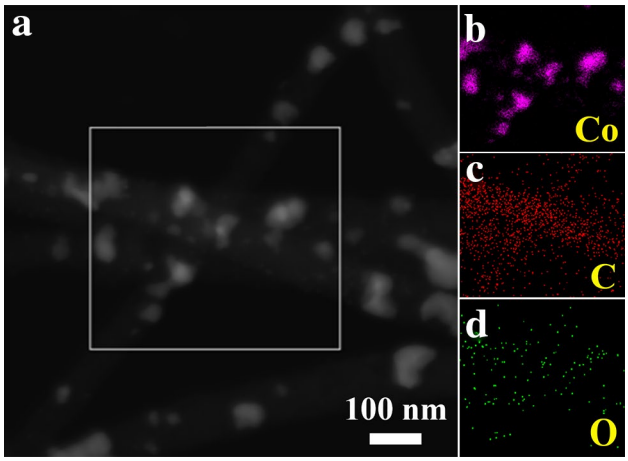

Fig. 5 STEM-HAADF image of S750 (**a**) and EDX mapping images of Co (**b**), C (**c**) and O (**d**) elements, respectively

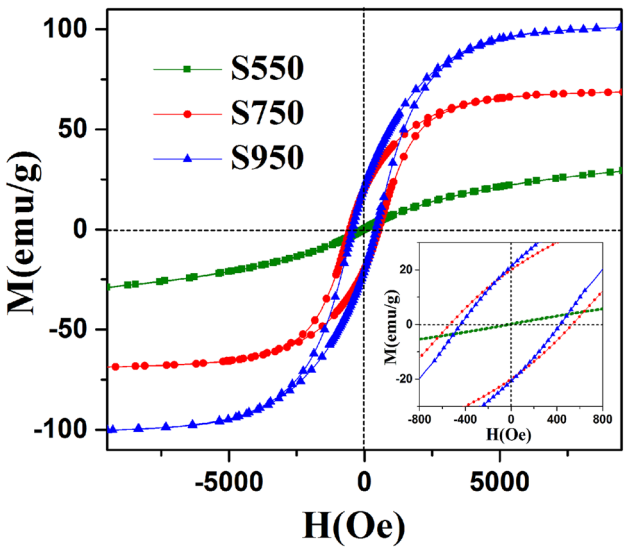

Fig. 6 Hysteresis loops of S550, S750 and S950. The inset shows an enlarged view of magnetization of these samples

weak magnetism of the S550 sample. While for S750 and S950, their saturation magnetizations (Ms) are 68.4 emu/g and 100.8 emu/g, respectively. In comparison, the Ms of bulk Co is 162.6 emu/g, much higher than that of Co-C NFs resulting from the 1D structure in NFs and the existence of nonmagnetic carbon [32]. Meanwhile, the inset of Fig. 6 indicates that the retentivity magnetization (Mr) of S750 and S950 are ca. 19.9 emu/g and 21.3 emu/g, respectively. In addition, the coercivity (Hc) values of Co-C NFs are ca. 529.6 Oe and 428.5 Oe for S750 and S950, respectively, much higher than the Hc value of bulk Co of 10.0 Oe [34]. The enhancement of Hc might be contributed by the surface anisotropy, single-domain characteristics and good dispersion of the NFs [35].

3.3 Electromagnetic parameters of Co-C NFs

The microwave absorption performance of the paraffin composites that contain 10 wt% Co-C NFs is greatly related to their complex permittivity and complex permeability, where the imaginary parts (ε″ and μ″) and real parts (ε′ and μ′) represent the loss and storage capability of EM energy, respectively. Figure 7 shows the EM parameters of all samples. The ε′ and ε″ values of S550, S750 and S950 at 2.0–18.0 GHz are exhibited in Fig. 7a, c, respectively. It can be seen that the ε′ value decreases from 5.6 to 2.9, 22.9 to 12.5 and 16.5 to 11.8 for S550, S750 and S950, respectively. The ε˝ values of S550, S750 and S950 gradually change from 4.3 to 1.2, 7.9 to 8.3 and 3.4 to 6.3, respectively. It can be found that the complex permittivity of Co-C NFs first increases and then decreases as the carbonization temperature increases from 550 °C to 950 °C, which could be explained by two aspects. On one side, based on free electron theory [3], the complex permittivity decreases with the material's conductivity decreasing. Therefore, the formation of too many defects in S550 could lead to the reduction in the conductivity of the Co-C NFs, which further result in reduced complex permittivity. On the other side, the permittivity of metal Co is lower than that of carbon [36]. Hence, more metal Co formed in S950 would reduce the permittivity of the Co-C NFs. Figure 7b, d exhibit the μ′ and μ″ values of S550, S750 and S950 at 2.0–18.0 GHz, respectively. As indicated by the figures, the curves of all samples show large fluctuation, probably resulting from the eddy currents contributed by the nanoscale Co-C NFs [29]. The curves of S950 and S750 display the optimal and worst complex permeability, respectively. In addition, Fig. 7e, f indicate that the dielectric loss tangent ($\tan \delta_\varepsilon = \varepsilon''/\varepsilon'$) is greater than the magnetic loss tangent ($\tan \delta_\mu = \mu''/\mu'$) in the measured frequency for all samples, revealing that the EM wave loss of the Co-C NFs is mainly attributed to the dielectric loss. In addition, the $\tan \delta_\varepsilon$ curves with two weak peaks reveal that the process of microwave loss exists in the dual dielectric relaxation. Besides, for all samples, the values of $\tan \delta_\mu$ nearly equal the values of μ″. By contrast, the μ″ of the three samples with two peaks at 6.3 GHz and 12.0 GHz are lower than 0.06 and show negative values at some frequency, with a minimum value of −0.11. Markel et al. presented that the value of μ″ could be negative in diamagnetic [37], while the Co-C NFs are ferromagnetic according to the VSM results. Negative μ″ could be obtained by implicit Fabry-Pérot resonance for composites and high loss dielectrics based on previous research [38, 39]. As observed in Fig. 7c, e, the Co-C NFs/paraffin composites should be regarded as high loss dielectrics according to Hou et al. [40]. As a result, the negative value may be due to the Fabry-Pérot resonance of Co-C NFs/paraffin composites. The Negative μ″ values of diverse composites are shown in Table 1.

Based on Debye theory, the relationship between ε″ and ε′ is expressed as [28]:

$$\left(\varepsilon' - \frac{\varepsilon_s + \varepsilon_\infty}{2}\right)^2 + (\varepsilon'')^2 = \left(\frac{\varepsilon_s - \varepsilon_\infty}{2}\right)^2 \quad (6)$$

where ε_∞ and ε_s are the relative dielectric permittivity and static permittivity at high-frequency limit, respectively.

As a result, the relationship between ε′ and ε″ show a pattern of single semicircle, i.e. Cole–Cole semicircle, and one Debye relaxation process corresponds to each semicircle. To clarify the influence of carbonization temperature on the Debye dielectric relaxation model of Co-C NFs, the dielectric relaxation mechanisms are investigated. Figure 7g shows the relationship between ε′ and ε″ for all samples. No obvious semicircle is observed in the curve of S550, indicating that the Debye relaxation is not prominent in S550. Meanwhile, two semicircles are observed in the curves of S750 and S950, suggesting the presence of dual dielectric relaxation processes in these two samples [42]. In addition, two weak semicircles are observed in the curve of S750, and the distinct semicircle is found in the curve of S950, suggesting stronger dual Debye relaxation effect on the permittivity of S950 than on that of S750 [42].

Polarization loss is an important form of dielectric loss, mainly involving ion polarization, interface polarization, electron polarization and dipole orientation polarization [24]. However, electron polarization and ion polarization are excluded as they usually take place at the frequency of 10^3–10^6 GHz. Meanwhile, dipole orientation polarization mainly results from the dipole redirection and the EM field interaction, and interface polarization results from the charge distribution at heterogeneous interfaces [43]. Consequently, we can conclude that the dielectric loss of Co-C NFs mainly results from interface polarization and dipole orientation polarization. On one side, the charge transfer between the carbon, Co and CoO could lead to interface polarization. On the other side, the dipole orientation polarization is caused

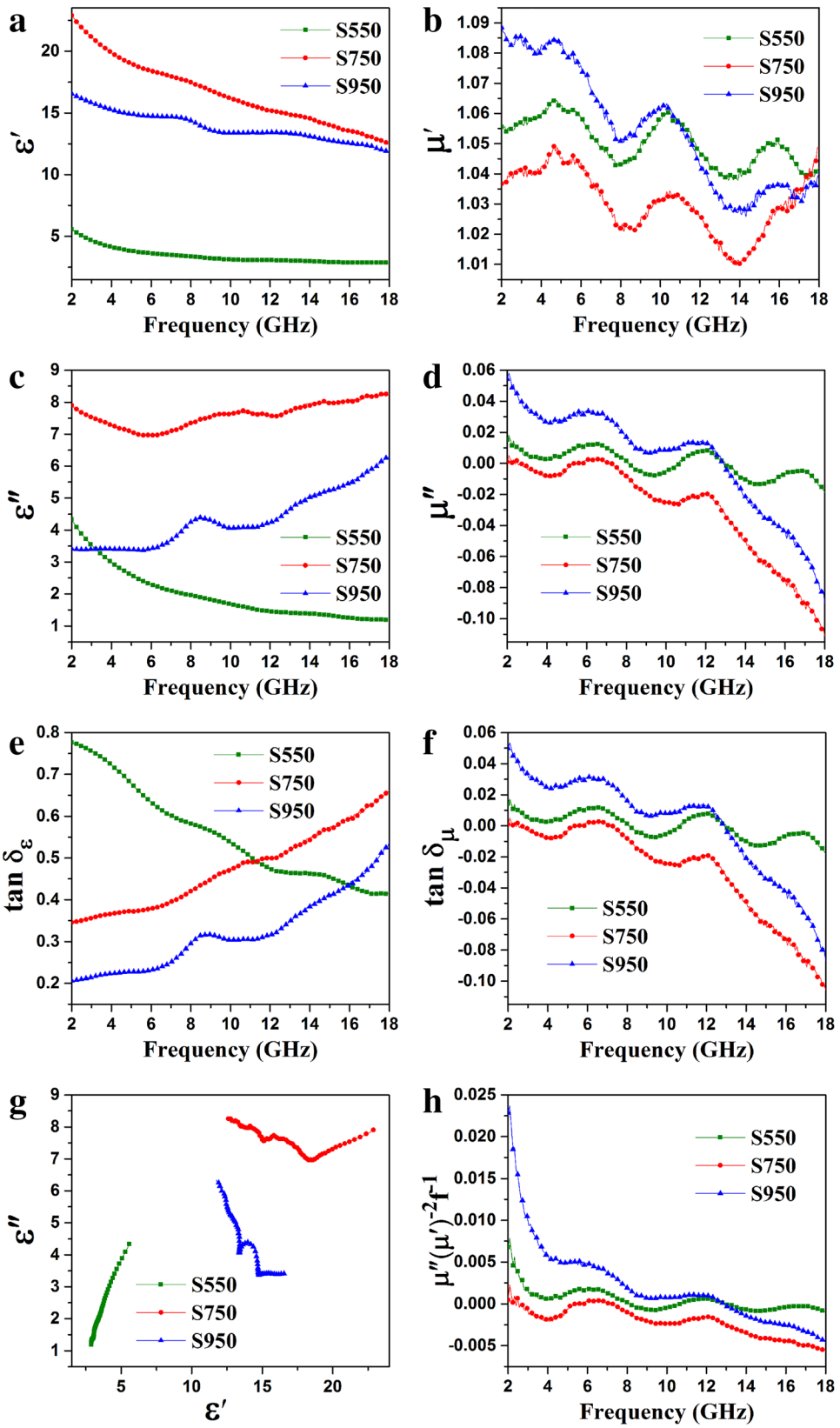

Fig. 7 Frequency dependences of the real (**a**) and imaginary (**c**) parts of the complex permittivity, real (**b**) and imaginary (**d**) part of the complex permeability, the dielectric loss tangent (**e**) and magnetic loss tangent (**f**), $\mu''(\mu')^{-2}f^{-1}$ (**h**), and Cole – Cole semicircles (ε' versus ε'') (**g**) for S550, S750 and S950

Table 1 Negative μ″ values of diverse composites

Materials	The minimum value of μ″	Ref.
C-wrapped Ni composites	−0.05	[17]
Ni-C nanofibers	−0.06	[33]
Fe/C porous nanofibers	−0.20	[39]
C/Co nanofibers	−0.05	[41]
Co-C nanofibers	−0.11	Herein

by the electric dipoles generated from the defects in the Co-C NFs.

In addition to the dielectric loss, magnetic loss also plays a critical role in influencing the microwave absorption performance. Magnetic loss mainly involves exchange resonance, natural resonance, eddy current loss, hysteresis loss and domain wall resonance [44]. Specifically, domain wall resonance usually occurs at the frequency of 1–100 MHz, and the hysteresis loss from irreversible magnetization can be excluded under the condition of a weak field. Eddy current loss is associated with the electric conductivity (σ) and sample thickness (d), which is expressed as [3]:

$$\mu'' = 2\pi\mu_0(\mu')^2\sigma * d^2 f/3 \tag{7}$$

where f and μ_0 represent the frequency and the permeability in vacuum, respectively. Thus, $\mu''(\mu')^{-2}f^{-1}$ can be expressed as

$$\mu''(\mu')^{-2}f^{-1} = 2\pi\mu_0\sigma d^2/3 \tag{8}$$

We all know that if magnetic loss is solely caused by eddy current loss, $\mu''(\mu')^{-2}f^{-1}$ is a constant value. Nevertheless, Fig. 7h shows that there are two peaks in $\mu''(\mu')^{-2}f^{-1} - f$ curves, meaning that the contribution of eddy current loss is excluded. As a result, we can conclude that natural resonance and exchange resonance contribute mostly to magnetic loss. Thus, for all the samples, the resonance peaks at 6.2 GHz are caused by the natural resonance, while the resonance peaks at 11.9 GHz are attributed to the exchange resonance according to Aharoni's theory [45].

3.4 Microwave absorption properties

To evaluate the EM wave absorption performance of the three samples, the RL was calculated according to transmission line theory, as expressed by [46, 47]:

$$\varepsilon_r = \varepsilon' - j\varepsilon'' \tag{9}$$

$$\mu_r = \mu' - j\mu'' \tag{10}$$

$$Z_{in} = Z_0\sqrt{\frac{\mu_r}{\varepsilon_r}}\tanh\left[j\left(\frac{2\pi fd}{c}\right)\sqrt{\mu_r\varepsilon_r}\right] \tag{11}$$

$$\mathrm{RL(dB)} = 20\log\left|\frac{Z_{in} - Z_0}{Z_{in} + Z_0}\right| \tag{12}$$

where Z_0 represents the free space impedance, Z_{in} is the input characteristic impedance, μ_r is the permeability, d means the absorber thickness, ε_r means the complex permittivity, c is the light velocity and f is the microwave frequency.

Evaluation is performed on the microwave absorption performance of all samples according to the permittivity and relative permeability at 2.0–18.0 GHz with different absorber thicknesses. Figure 8 shows the RL curves of S550, S750 and S950. For S550, the minimum RL is −26.7 dB at 7.9 GHz with a thickness of 5.0 mm. For S750, the minimum RL is −19.6 dB at 4.2 GHz with a thickness of 3.5 mm. For S950, the optimal minimum RL is −33.1 dB at 14.1 GHz with a thickness of 1.5 mm and the effective bandwidth of absorption is 4.1 GHz (from 12.3 GHz to 16.4 GHz) for RL ≤ −10 dB. The RL values are transformed into color maps to visualize the relationship between RL, matched thickness and frequency width. Figure 9 presents the RL color maps of the three samples at the frequency of 2.0–18.0 GHz and with a thickness of 1.0–5.0 mm. As shown in Fig. 9, the minimum RL gradually moves to the

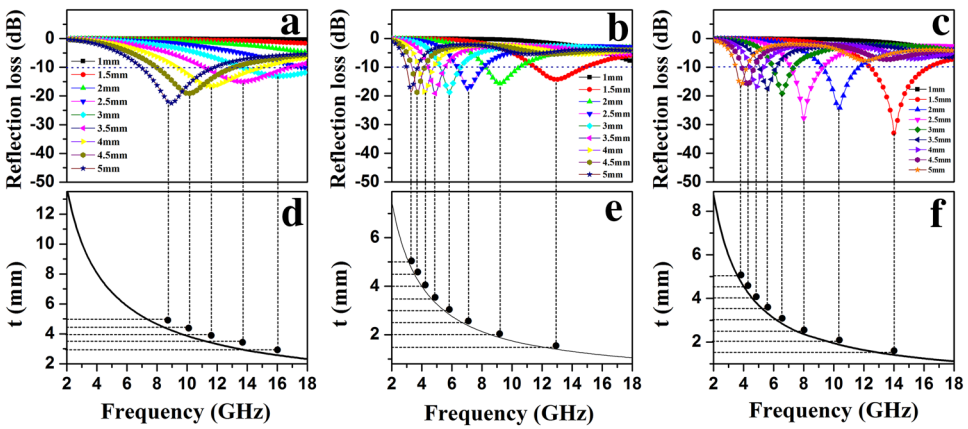

Fig. 8 Frequency dependence of the reflection loss curves for S550 (**a**), S750 (**b**) and S950 (**c**); Simulations of the absorber thickness (t_m) versus peak frequency (f_m) for S550 (**d**), S750 (**e**) and S950 (**f**) under the λ/4 model

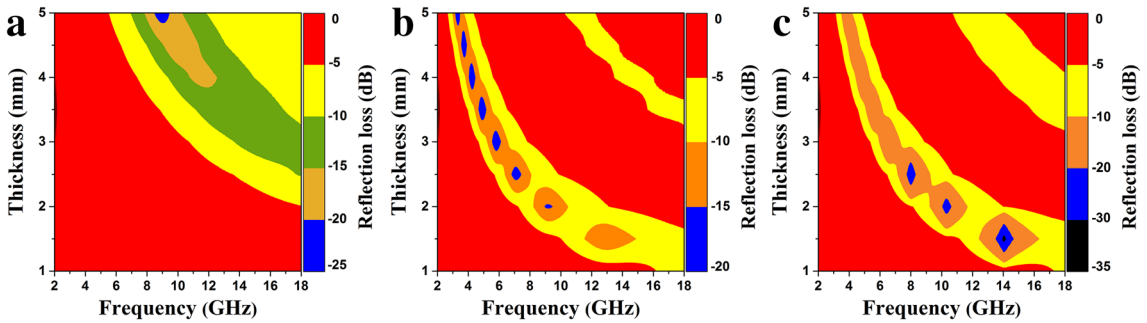

Fig. 9 Reflection loss maps in the frequency range of 2.0–18.0 GHz with varied absorber thickness from 1.0 to 5.0 mm for S550 (**a**), S750 (**b**) and S950 (**c**)

low-frequency range as the thickness increases. It should be noted that S950 shows great advantages in all three aspects of the three samples. On one side, moderate complex permittivity has more benefits for improving the performance of an EM wave absorber than a lower or higher one [36]. On the other side, the optimal complex permeability plays a key role in optimizing impedance matching. Therefore, the introduction of controlled magnetic Co nanoparticles can dramatically optimize impedance matching, improve the magnetic loss, and eventually lead to good microwave absorption performance.

Apart from the influence from impedance matching and electromagnetic loss, microwave absorption performance is also affected by the quarter-wavelength matching model ($\lambda/4$ model). When the matching frequency shifts to the low-frequency range, the absorber's thickness correspondingly increases, which can be preliminarily explained by the $\lambda/4$ model [48]. Then, the relationship between the frequency of peak and absorber thickness is given by [49]:

$$t_m = \frac{n\lambda}{4} = \frac{nc}{4f_m\sqrt{|\mu_r||\varepsilon_r|}} \tag{13}$$

where t_m represents the matching layer thickness, λ means the microwave wavelength, $|\mu_r|$ and $|\varepsilon_r|$ represent the modulus of the μ_r and ε_r, respectively, c is the light speed, f_m represents the frequency and n is the uneven number. Based on the $\lambda/4$ model, the two newly-generated reflection microwaves from the interfaces of absorber–metal and absorber–air are out of phase by 180° when the absorber thickness obeys Eq. (13), resulting in the interference cancellation of EM waves at the interface of air–absorber. Figure 8 shows that all the RL peaks of the three samples well coincide with the $\lambda/4$ model when the sample thicknesses change from 1.0 mm to 5.0 mm, indicating that the $\lambda/4$ model is confirmed by the low-frequency absorbing characteristics of all samples [42].

It is generally considered that an excellent absorber should possess two essential features, i.e. impedance matching and the attenuation of EM wave within an absorber [50]. $Z=|Z_{in}/Z_0|$ can be calculated by Eq. (11) for evaluating impedance matching. When $Z=|Z_{in}/Z_0|$ is close to 1, that is, Z_{in} is close to Z_0, absorbers will achieve an optimal impedance matching with free space, suggesting no reflection on the absorber-air interface. Figure 10 displays the dependences of color maps of Z values on the frequency at absorber thicknesses of 1.0–5.0 mm. Black dotted lines represent the Z values that are close to 1 (between 0.8 and 1.2). It can be clearly seen that the Z values of S950 close to 1 covered a relatively broad frequency for absorber's thickness less than 2.0 mm, indicating the better impedance matching of S950.

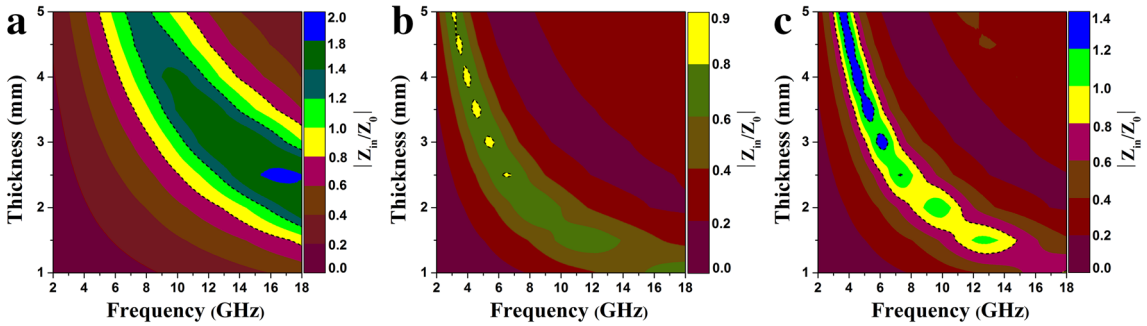

Fig. 10 Color maps of Z values in the frequency range of 2.0–18.0 GHz with varied absorber thickness from 1.0 mm to 5.0 mm for S550 (**a**), S750 (**b**) and S950 (**c**)

The EM wave absorption performance over the measured frequency range can be adjusted by altering the matching thickness. The improvement in the EM wave impedance matching can be indicated by two aspects. One aspect is the synergistic effect between dielectric loss materials and magnetic loss materials, and the other aspect is the 1D nanostructure of carbon fibers assembled by Co nanoparticles.

In addition, attenuation constant α is another critical factor for evaluating the microwave absorption performance. The attenuation constant is given by [50]:

$$\alpha = \frac{\sqrt{2}\pi f}{c} \times \sqrt{(\mu''\varepsilon'' - \mu'\varepsilon') + \sqrt{(\mu''\varepsilon'' - \mu'\varepsilon')^2 + (\mu'\varepsilon'' + \mu''\varepsilon')^2}} \quad (14)$$

where f represents the frequency and c means the microwave speed in free space.

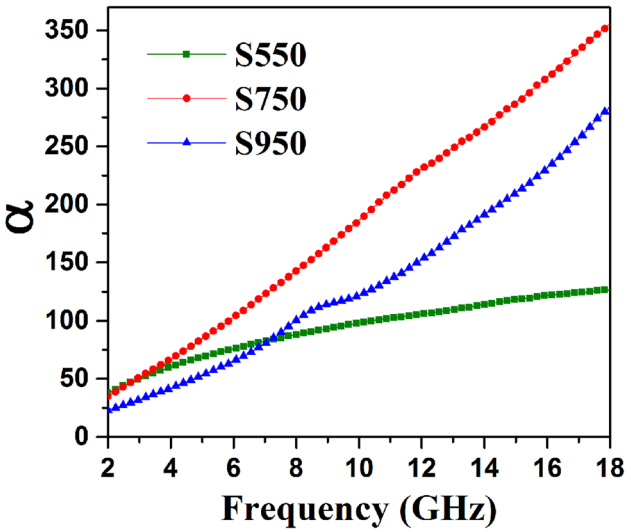

Fig. 11 Frequency dependences of the attenuation constant for S550, S750 and S950

Figure 11 presents the frequency dependences of the attenuation constant α for S550, S750 and S950. The α value of S750 is greater than that of S950 and S550, indicating that S750 has better attenuation ability for microwaves than the other two. However, S750 exhibits the poorest microwave absorption performance resulting from its worst impedance matching. Meanwhile, S950 displays moderate attenuation ability for microwaves, but exhibits the optimal RL due to the better impedance matching. These findings are helpful for preparing EM wave absorbers with excellent absorption performance. Both the EM wave attenuation ability and impedance matching should be considered.

Figure 12 illustrates a possible mechanism of Co-C NFs absorbing microwave. Firstly, the formulation of a conductive network by Co-C NFs could improve the EM wave absorption performance. Secondly, the microwave scattering generated in Co-C NFs can enhance the attenuation of EM waves. Thirdly, the charge transfer between carbon, CoO, Co, and graphene layers could give rise to the electric dipoles formation and lead to the generation of dipole orientation polarization and interface polarization, which could further increase the dielectric loss. Finally, the magnetic loss resulting from magnetic Co and CoO nanoparticles is able to optimize the impedance matching, further increasing the EM wave absorption performance. The lower loading ratio in paraffin composite and good EM wave absorption properties of Co-C NFs can be displayed in Table 2 compared with other Co-C absorbers.

3.5 Superhydrophobic properties

The superhydrophobic property of EM wave absorbers is quite significant for their military and civilian applications. The hydrophobicity of all samples was investigated by measuring the water CA on the Co-C NFs membrane. Figure 13 shows a drop of water on the membrane of S550, S750 and S950, with the CA being 139°, 150° and 152°, respectively.

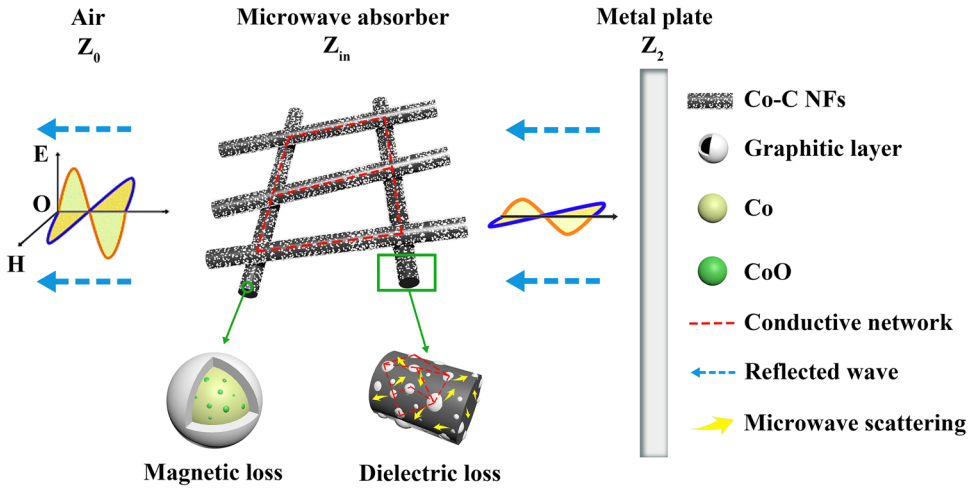

Fig. 12 Schematic representation of the microwave absorption mechanism for Co-C NFs

Table 2 EM wave absorption properties of diverse Co-C composites

Absorbers	Loading ratio in paraffin composite (wt %)	d (mm)	RL_{min} (dB)	f_m (GHz)	f_e (GHz) (RL < − 10 dB)	Ref.
Co/porous C composites	25	3.0	− 30.3	11.0	4.9	[24]
Co/C nanoparticles	50	2.3	− 43.4	16.8	7.2	[29]
Co@C microspheres	70	1.7	− 68.7	10.6	15.3	[51]
Co/C fibers	33	2.5	− 24.6	14.2	6.7	[52]
Co/C microspheres	30	2.0	− 31.3	12.8	4.4	[53]
Co-C NFs	10	1.5	− 33.1	14.1	4.1	Herein

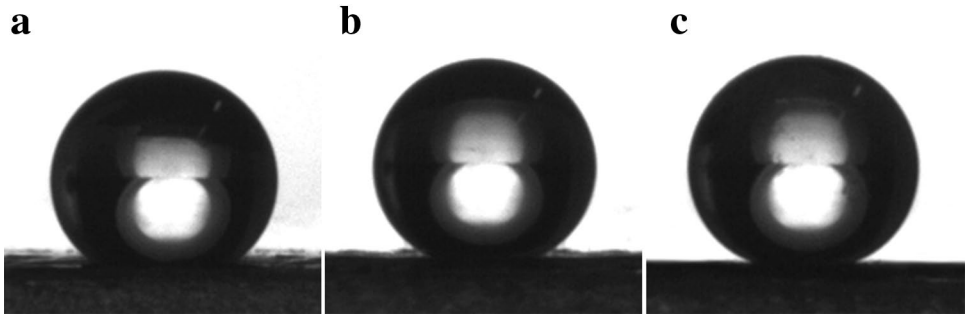

Fig. 13 Optical images of water droplets on membranes of S550 (**a**), S750 (**b**) and S950 (**c**)

Therefore, the as-prepared S750 and S950 samples exhibit the superhydrophobic property in the air. In addition, the CA of the S550 sample is smaller than 150° due to the lower surface roughness. Hence, the hydrophobicity of Co-C NFs can be changed by adjusting the calcination temperature. With the excellent superhydrophobic property and microwave absorption performance, the prepared Co-C NFs composites can be potentially applied to stealth materials.

4 Conclusions

The Co-C NFs were fabricated using electrospinning method with the different carbonization temperatures of 550 °C, 750 °C and 950 °C in vacuum. The morphologies and structures of the as-prepared composites could be artificially controlled. The generated Co nanoparticles were uniformly distributed along the NFs and their amount increased as the calcination temperature increased. The microwave absorption performance of all samples, i.e. S550, S750 and S950, was evaluated using the transmission/reflection method. It was found that the paraffin composites containing only 10 wt% Co-C NFs calcined at 950 °C displayed the best EM wave absorption performance. For this case, the optimal RL reached − 33.1 dB at 14.1 GHz with a thickness of 1.5 mm, and the effective bandwidth of absorption was 4.1 GHz (from 12.3 GHz to 16.4 GHz) for RL ≤ − 10 dB. Besides, the dielectric loss of Co-C NFs was mainly caused by dipole orientation polarization and interface polarization. The magnetic loss mainly resulted from the natural resonance and exchange resonance. In addition, the as-prepared S750 and S950 membranes exhibited the superhydrophobic property in the air. Thus, these lightweight Co-C NFs composites have potential applications to producing water-resistant stealthy materials.

Acknowledgements This work was supported by the National Natural Science Foundation of China (No. 51363015) and the Gansu Province Natural Science Foundation (No. 1506RJZA107).

References

1. W. She, H. Bi, Z. Wen, Q. Liu, X. Zhao, J. Zhang, R. Che, Tunable microwave absorption frequency by aspect ratio of hollow polydopamine@alpha-MnO_2 microspindles studied by electron holography. ACS Appl. Mater. Interfaces **8**, 9782–9789 (2016)
2. Q. Liu, Q. Cao, H. Bi, C. Liang, K. Yuan, W. She, Y. Yang, R. Che, CoNi@SiO_2@TiO_2 and CoNi@Air@TiO_2 microspheres with strong wideband microwave absorption. Adv. Mater. **28**, 486–490 (2016)
3. Y. Du, W. Liu, R. Qiang, Y. Wang, X. Han, J. Ma, P. Xu, Shell thickness-dependent microwave absorption of core-shell Fe_3O_4@C composites. ACS Appl. Mater. Interfaces **6**, 12997–13006 (2014)
4. J. Feng, F. Pu, Z. Li, X. Li, X. Hu, J. Bai, Interfacial interactions and synergistic effect of CoNi nanocrystals and nitrogen-doped graphene in a composite microwave absorber. Carbon **104**, 214–225 (2016)
5. W. Chu, Y. Wang, Y. Du, R. Qiang, C. Tian, X. Han, FeCo alloy nanoparticles supported on ordered mesoporous carbon for enhanced microwave absorption. J. Mater. Sci. **52**, 13636–13649 (2017)
6. H. Wu, G. Wu, Y. Ren, L. Yang, L. Wang, X. Li, Co^{2+}/Co^{3+} ratio dependence of electromagnetic wave absorption in hierarchical

$NiCo_2O_4$-$CoNiO_2$ hybrids. J. Mater. Chem. C **3**, 7677–7690 (2015)
7. Y. Cheng, M. Tan, P. Hu, X. Zhang, B. Sun, L. Yan, S. Zhou, W. Han, Strong and thermostable SiC nanowires/graphene aerogel with enhanced hydrophobicity and electromagnetic wave absorption property. Appl. Surf. Sci. **448**, 138–144 (2018)
8. H. Wang, Y. Zheng, W. Cui, Y. Sun, D. Zhang, Interface polarization strategy to prepare Sn/SnO_2@C absorber with tunable core compositions and broader frequency absorption properties. Appl. Surf. Sci. **455**, 1057–1062 (2018)
9. D. Lan, M. Qin, R. Yang, S. Chen, H. Wu, Y. Fan, Q. Fu, F. Zhang, Facile synthesis of hierarchical chrysanthemum-like copper cobaltate-copper oxide composites for enhanced microwave absorption performance. J Colloid Interface Sci. **533**, 481–491 (2019)
10. M. Qiao, X. Lei, Y. Ma, L. Tian, K. Su, Q. Zhang, Dependency of tunable microwave absorption performance on morphology-controlled hierarchical shells for core-shell Fe_3O_4@MnO_2 composite microspheres. Chem. Eng. J. **304**, 552–562 (2016)
11. H. Wu, S. Qu, K. Lin, Y. Qing, L. Wang, Y. Fan, Q. Fu, F. Zhang, Enhanced low-frequency microwave absorbing property of SCFs@TiO_2 composite. Powder Technol. **333**, 153–159 (2018)
12. C. Song, X. Yin, M. Han, X. Li, Z. Hou, L. Zhang, L. Cheng, Three-dimensional reduced graphene oxide foam modified with ZnO nanowires for enhanced microwave absorption properties. Carbon **116**, 50–58 (2017)
13. P. Liu, Y. Huang, J. Yan, Y. Yang, Y. Zhao, Construction of CuS nanoflakes vertically aligned on magnetically decorated graphene and their enhanced microwave absorption properties. ACS Appl. Mater. Interfaces **8**, 5536–5546 (2016)
14. M. Yu, C. Liang, M. Liu, X. Liu, K. Yuan, H. Cao, R. Che, Yolk-shell Fe_3O_4@ZrO_2 prepared by a tunable polymer surfactant assisted sol–gel method for high temperature stable microwave absorption. J. Mater. Chem. C **2**, 7275–7283 (2014)
15. G. Wu, Y. Cheng, Y. Ren, Y. Wang, Z. Wang, H. Wu, Synthesis and characterization of gamma-Fe_2O_3@C nanorod-carbon sphere composite and its application as microwave absorbing material. J. Alloys Compd. **652**, 346–350 (2015)
16. Z. Qiu, Y. Peng, D. He, Y. Wang, S. Chen, Ternary Fe_3O_4@C@PANi nanocomposites as high-performance supercapacitor electrode materials. J. Mater. Sci. **53**, 12322–12333 (2018)
17. W. Liu, Q. Shao, G. Ji, X. Liang, Y. Cheng, B. Quan, Y. Du, Metal–organic-frameworks derived porous carbon-wrapped Ni composites with optimized impedance matching as excellent lightweight electromagnetic wave absorber. Chem. Eng. J. **313**, 734–744 (2017)
18. Y. Wang, Y. Du, D. Guo, R. Qiang, C. Tian, P. Xu, X. Han, Precursor-directed synthesis of porous cobalt assemblies with tunable close-packed hexagonal and face-centered cubic phases for the effective enhancement in microwave absorption. J. Mater. Sci. **52**, 4399–4411 (2016)
19. Y. Hou, L. Cheng, Y. Zhang, Y. Yang, C. Deng, Z. Yang, Q. Chen, P. Wang, L. Zheng, Electrospinning of Fe/SiC hybrid fibers for highly efficient microwave absorption. ACS Appl. Mater. Interfaces **9**, 7265–7271 (2017)
20. Y. Pang, X. Xie, D. Li, W. Chou, T. Liu, Microporous Ni@NiO nanoparticles prepared by chemically dealloying Al_3Ni_2@Al nanoparticles as a high microwave absorption material. J. Magn. Magn. Mater. **426**, 211–216 (2017)
21. J. Deng, X. Zhang, B. Zhao, Z. Bai, S. Wen, S. Li, S. Li, J. Yang, R. Zhang, Fluffy microrods to heighten the microwave absorption properties through tuning the electronic state of Co/CoO. J. Mater. Chem. C **6**, 7128–7140 (2018)
22. H. Wu, G. Wu, L. Wang, Peculiar porous alpha-Fe_2O_3, gamma-Fe_2O_3 and Fe_3O_4 nanospheres: Facile synthesis and electromagnetic properties. Powder Technol. **269**, 443–451 (2015)
23. H. Pang, A.M. Abdalla, R.P. Sahu, Y. Duan, I.K. Puri, Low-temperature synthesis of manganese oxide–carbon nanotube-enhanced microwave-absorbing nanocomposites. J. Mater. Sci. **53**, 16288–16302 (2018)
24. H. Wang, L. Xiang, W. Wei, J. An, J. He, C. Gong, Y. Hou, Efficient and lightweight electromagnetic wave absorber derived from metal organic framework-encapsulated cobalt nanoparticles. ACS Appl. Mater. Interfaces **9**, 42102–42110 (2017)
25. X.H. Li, J. Feng, Y.P. Du, J.T. Bai, H.M. Fan, H.L. Zhang, Y. Peng, F.S. Li, One-pot synthesis of $CoFe_2O_4$/graphene oxide hybrids and their conversion into FeCo/graphene hybrids for lightweight and highly efficient microwave absorber. J. Mater. Chem. A **3**, 5535–5546 (2015)
26. C. Sun, Y. Guo, X. Xu, Q. Du, H. Duan, Y. Chen, H. Li, H. Liu, In situ preparation of carbon/Fe_3C composite nanofibers with excellent electromagnetic wave absorption properties. Compos. Part A **92**, 33–41 (2017)
27. G. Wang, Z. Gao, S. Tang, C. Chen, F. Duan, S. Zhao, S. Lin, Y. Feng, L. Zhou, Y. Qin, Microwave absorption properties of carbon nanocoils coated with highly controlled magnetic materials by atomic layer deposition. ACS Nano **6**, 11009–11017 (2012)
28. Y. Zhang, X. Zhang, B. Quan, G. Ji, X. Liang, W. Liu, Y. Du, A facile self-template strategy for synthesizing 1D porous Ni@C nanorods towards efficient microwave absorption. Nanotechnology **28**, 115704 (2017)
29. T. Liu, X.B. Xie, Y. Pang, S. Kobayashi, Co/C nanoparticles with low graphitization degree: a high performance microwave-absorbing material. J. Mater. Chem. C **4**, 1727–1735 (2016)
30. X. Lu, Y. Wu, H. Cai, X. Qu, L. Ni, C. Teng, Y. Zhu, L. Jiang, Fe_3O_4 nanopearl decorated carbon nanotubes stemming from carbon onions with self-cleaning and microwave absorption properties. RSC Adv. **5**, 54175–54181 (2015)
31. Y. Li, Y. Zhao, X. Lu, Y. Zhu, L. Jiang, Self-healing superhydrophobic polyvinylidene fluoride/Fe_3O_4@polypyrrole fiber with core–sheath structures for superior microwave absorption. Nano Res. **9**, 2034–2045 (2016)
32. N.A.M. Barakat, B. Kim, S.J. Park, Y. Jo, M.-H. Jung, H.Y. Kim, Cobalt nanofibers encapsulated in a graphite shell by an electrospinning process. J. Mater. Chem. **19**, 7371 (2009)
33. Y. Shen, Y. Wei, J. Ma, Q. Li, J. Li, W. Shao, P. Yan, G. Huang, X. Du, Tunable microwave absorption properties of nickel-carbon nanofibers prepared by electrospinning. Ceram. Int. **45**, 3313–3324 (2019)
34. H. Wu, R. Zhang, X. Liu, D. Lin, W. Pan, Electrospinning of Fe, Co, and Ni nanofibers: synthesis, assembly, and magnetic properties. Chem. Mater. **19**, 3506–3511 (2007)
35. L. Sun, C.L. Chien, P.C. Searson, Fabrication of nanoporous nickel by electrochemical dealloying. Chem. Mater. **16**, 3125–3129 (2004)
36. G. Pan, J. Zhu, S. Ma, G. Sun, X. Yang, Enhancing the electromagnetic performance of Co through the phase-controlled synthesis of hexagonal and cubic Co nanocrystals grown on graphene. ACS Appl. Mater. Interfaces **5**, 12716–12724 (2013)
37. V.A. Markel, Can the imaginary part of permeability be negative?. Phys. Rev. E 78, (2008)
38. M. Maglione, M.A. Subramanian, Dielectric and polarization experiments in high loss dielectrics: a word of caution. Appl. Phys. Lett. 93, (2008)
39. F. Wang, Y. Sun, D. Li, B. Zhong, Z. Wu, S. Zuo, D. Yan, R. Zhuo, J. Feng, P. Yan, Microwave absorption properties of 3D cross-linked Fe/C porous nanofibers prepared by electrospinning. Carbon **134**, 264–273 (2018)
40. Z.L. Hou, M. Zhang, L.B. Kong, H.M. Fang, Z.J. Li, H.F. Zhou, H.B. Jin, M.S. Cao, Microwave permittivity and permeability experiments in high-loss dielectrics: caution with implicit

fabry-perot resonance for negative imaginary permeability. Appl. Phys. Lett. 103, (2013)
41. X.K. Zhang, J. Xiang, Z.P. Wu, M. Liu, X.Q. Shen, Co content on absorption property of C/Co nanofibers as a lightweight microwave absorber. J. Inorg. Mater. **32**, 1299–1307 (2017)
42. T. Wu, Y. Liu, X. Zeng, T. Cui, Y. Zhao, Y. Li, G. Tong, Facile hydrothermal synthesis of Fe_3O_4/C Core–Shell nanorings for efficient low-frequency microwave absorption. ACS Appl. Mater. Interfaces **8**, 7370–7380 (2016)
43. C. Tian, Y. Du, P. Xu, R. Qiang, Y. Wang, D. Ding, J. Xue, J. Ma, H. Zhao, X. Han, Constructing uniform Core–Shell PPy@PANI composites with tunable shell thickness toward enhancement in microwave absorption. ACS Appl. Mater. Interfaces **7**, 20090–20099 (2015)
44. M. Qiao, X. Lei, Y. Ma, L. Tian, W. Wang, K. Su, Q. Zhang, Facile synthesis and enhanced electromagnetic microwave absorption performance for porous core-shell Fe_3O_4@MnO_2 composite microspheres with lightweight feature. J. Alloys Compd. **693**, 432–439 (2017)
45. A. Aharoni, Exchange resonance modes in a ferromagnetic sphere. J. Appl. Phys. **69**, 7762–7764 (1991)
46. X. Jian, B. Wu, Y. Wei, S.X. Dou, X. Wang, W. He, N. Mahmood, Facile synthesis of Fe_3O_4/GCs composites and their enhanced microwave absorption properties. ACS Appl. Mater. Interfaces **8**, 6101–6109 (2016)
47. X. Wang, B. Zhang, W. Zhang, M. Yu, L. Cui, X. Cao, J. Liu, Super-light Cu@Ni nanowires/graphene oxide composites for significantly enhanced microwave absorption performance. Sci. Rep. **7**, 1584 (2017)
48. X. Zheng, J. Feng, Y. Zong, H. Miao, X. Hu, J. Bai, X. Li, Hydrophobic graphene nanosheets decorated by monodispersed superparamagnetic Fe_3O_4 nanocrystals as synergistic electromagnetic wave absorbers. J. Mater. Chem. C **3**, 4452–4463 (2015)
49. Y. Lan, X. Li, Y. Zong, Z. Li, Y. Sun, G. Tan, J. Feng, Z. Ren, X. Zheng, In-situ synthesis of carbon nanotubes decorated by magnetite nanoclusters and their applications as highly efficient and enhanced microwave absorber. Ceram. Int. **42**, 19110–19118 (2016)
50. X. Zhang, G. Ji, W. Liu, X. Zhang, Q. Gao, Y. Li, Y. Du, A novel Co/TiO_2 nanocomposite derived from a metal-organic framework: synthesis and efficient microwave absorption. J. Mater. Chem. C **4**, 1860–1870 (2016)
51. D. Ding, Y. Wang, X. Li, R. Qiang, P. Xu, W. Chu, X. Han, Y. Du, Rational design of core-shell Co@C microspheres for high-performance microwave absorption. Carbon **111**, 722–732 (2017)
52. W. Li, H. Qi, F. Guo, Y. Du, N. Song, Y. Liu, Y. Chen, Co nanoparticles supported on cotton-based carbon fibers: a novel broadband microwave absorbent. J. Alloys Compd. **772**, 760–769 (2019)
53. Z. Li, X. Han, Y. Ma, D. Liu, Y. Wang, P. Xu, C. Li, Y. Du, MOFs-derived hollow Co/C microspheres with enhanced microwave absorption performance. Acs Sustain. Chem. Eng. **6**, 8904–8913 (2018)